Electrodeposited $Co_{93.2}P_{6.8}$ nanowire arrays with core-shell microstructure and perpendicular magnetic anisotropy

F. Nasirpouri[1,*] S.M. Peighambari[1], A.S. Samardak[2], A.V.Ognev[2], E.V. Sukovatitsina[2],

E.B. Modin[2], L.A. Chebotkevich[2], S.V. Komogortsev[3], S. Bending[4]

[1]*Faculty of Materials Engineering, Sahand University of Technology, Tabriz 51335-1996, Iran*

[2]*School of Natural Sciences, Far Eastern Federal University, Vladivostok, Russia*

[3]*Institute of Physics, SB Russian Academy of Sciences, Krasnoyarsk, 660036 Russia*

[4]*Department of Physics, University of Bath, Bath, UK*

Abstract

We demonstrate the formation of an unusual core-shell microstructure in $Co_{93.2}P_{6.8}$ nanowires electrodeposited by alternating current (ac) in an alumina template. By means of the transmission electron microscopy it is shown that the coaxial-like nanowires contains an amorphous and crystalline phases. Analysis of the magnetization data for Co-P alloy nanowires indicates that a ferromagnetic core is surrounded by a weakly ferromagnetic or non-magnetic phase, depending on the phosphor content. The nanowire arrays exhibit an easy axis of magnetization parallel to the wire axis. For this peculiar composition and structure, the coercivity values are 2380±50 and 1260±35 Oe in parallel and perpendicular to the plane directions of magnetization, respectively. This effect is attributed to the core-shell structure making the properties and applications of these nanowires similar to pure cobalt nanowires with an improved perpendicular anisotropy.

Keywords: AC electrodeposition, magnetic nanowires, magnetic anisotropy.

PACS: 81.15.Pq, 81.07.Gf, 75.30.Gw.

Introduction

Magnetic nanowires are known as an important category of nanoscale magnetic materials whose properties such as the domain wall width and magnetic exchange length have interesting physics and device applications [1]. Magnetization reversal mechanisms, switching fields, domain wall movement and interaction in magnetic nanowires have been studied in details [2-4]. The magnetic properties of arrays of elemental and alloyed ferromagnetic nanowires electrodeposited inside the void spaces of anodic aluminium oxide (AAO) and of polymer membranes have been extensively investigated. Because of different pore arrangements of each template, the consequent magnetic properties of nanowires are considerably influenced. Cobalt nanowires not only show the strong shape anisotropy, that can be observed for Fe and Ni wires, but also a temperature and size dependent magnetocrystalline anisotropy along the hexagonal c-axis of *hcp*-Co. This c-axis is known to be perpendicular to the long axis of the wire. It is well known that the *hcp* structure favors an easy magnetization axis being perpendicular to the wire length, while in the *fcc* phase the easy magnetization axis lies mainly parallel to the wire axis [5-11]. This decays the application of high coercivity cobalt nanowires for perpendicular applications.

In this work we demonstrate the formation of an unusual core-shell structure in Co-P nanowires with high coercivity values comparable to that of cobalt nanowires along with perpendicular to plane anisotropy [10,11]. Our interpretation for the coaxial core-shell structure of the Co-P nanowires, which were electrodeposited under a specific condition, is based on a careful analysis of experimental magnetization data, including hysteresis loops and magnetic torque measurements.

Experimental

High purity Al foils (99.999 wt.%) were used as substrates to fabricate highly ordered AAO templates using a two-step anodization process 40 V in a 0.3 M oxalic acid electrolyte at 0° C in both steps. At the end, the thickness of the barrier layer of oxide film was reduced by decreasing the anodizing voltage down to 12 V to facilitate electron transport at each reduction half-cycles. The diameter and length of nanopores were 30±3 nm and 5±0.3 μm, respectively. The interpore distance was 100±5 nm. Co-P alloy nanowires were then electrodeposited using alternating current (AC) at room temperature into the AAO templates in a two-electrode cell, where a stainless steel plate acts as a counter-electrode. The electrolyte consisted of 0.1 M $CoSO_4 \cdot 7H_2O$, 0.5 M boric acid and 0, 5, 15 and 25 g/liter NaH_2PO_2 at a pH close to 4. A sinusoidal waveform was employed with a voltage amplitude ranging from 12 to 15 V and a frequency ranging from 50 to 400 Hz. Prior to electrodeposition the AAO template was sonicated for 10 min in the electrolyte to facilitate wetting of the nanopores.

Field-emission scanning electron microscopy (SEM, Supra, Carl Zeiss), transmission electron microscopy (TEM, Libra, 200 Carl Zeiss), energy-dispersive X-ray spectroscopy (EDX, Oxford instruments), and X-ray diffraction (XRD, Bruker D8 Advanced, $Cu_{(K\alpha)}$ wavelength=0.1540496 nm) were used to investigate the morphology, chemical composition and microstructure of the samples. EDX was performed on the nanowires of the partially dissolved AAO template with one micron diameter of the scan area.

Magnetic hysteresis curves were recorded using a vibrating sample magnetometer (VSM Lake Shore 7407) in magnetic fields up to 12 kOe at room temperature. Samples were placed in parallel (normal to the long axis of the wires) and perpendicular (parallel to the long axis of the wires) geometries to the plane of the AAO template. The effect of magnetic signal coming from alumina substrate was eliminated from the hysteresis loops by subtracting the non-linearity after saturation using a method described in ref [12].

Results and discussion

The chemical composition of Co-P nanowires, electrodeposited from different bath phosphor contents, was analyzed using EDX. Magnetic parameters of nanowires, listed in Table 1 as a function of bath composition, are discussed below in the text.

Table 1. Phosphor content and the corresponding coercivity and saturation fields of Co-P nanowires electrodeposited with a 200Hz 15V sine wave from different composition solutions. ⊥ and || denote perpendicular and parallel directions to AAO substrate.

$NaH_2PO_2 \cdot H_2O$, g/litre	Phosphor content x, wt.%	Parallel coercivity $H_c(\|\|)$, Oe	Perpendicular coercivity $H_c(\perp)$, Oe	Parallel saturation field $H_s(\|\|)$, Oe	Perpendicular saturation field $H_s(\perp)$, Oe
0	0	330±20	865±30	9000±100	8600±100
5	6.8	1260±35	2380±50	8500±100	7000±100
15	8.2	920±30	1545±40	6800±80	6600±80
25	9.3	645±30	1005±40	5700±80	5600±80

XRD pattern of $Co_{100-x}P_x$ nanowires embedded in AAO and electrodeposited at 15 V and 200 Hz using the sinusoidal waveform is shown in Figure 1. For Co nanowires (x=0), *hcp* crystalline structure is observed with clear (001), (200) and (110) Bragg diffraction peaks. Co (200) peaks are overlapped with a Bragg peak belonging to the aluminum substrate. Aluminum peaks are annihilated in templates with higher filling fraction. The electrodeposited nanowires containing phosphor tend to lose crystallinity as (110) and (100) Bragg diffraction peaks disappear.

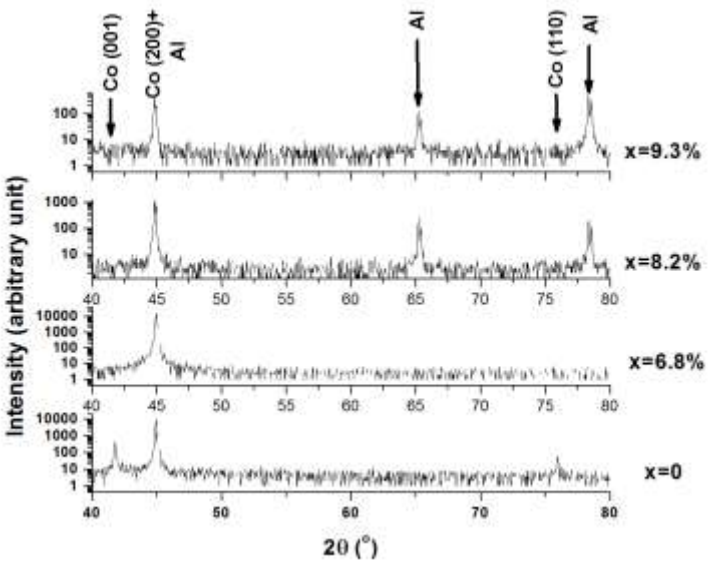

Figure 1 - X-ray diffraction patterns observed from an array of $Co_{100-x}P_x$ nanowires with different phosphor content (x) electrodeposited in AAO templates using (a) a 15V, 200Hz sinusoidal waveform from solutions containing 0, 5, 15 and 25 g/litre sodium hypophosphate.

The disappearance of the characteristic Bragg peaks alone is not enough to confirm the presence of an amorphous phase. As we discuss below, if just an amorphous phase was present only, a broad halo would be observed in selected area diffraction (SAED) patterns. However, we also observe bright diffraction spots corresponding to the presence of a polycrystalline phase. We attribute this observation to electrodeposition of Co-P nanowire arrays under non-equilibrium conditions, where the ratio between polycrystalline and amorphous phases is controlled by the P content.

Figure 2 shows the magnetic hysteresis loops measured for $Co_{100-x}P_x$ nanowires with *x*=0, 6.8 and 8.2 wt.% for an external magnetic field applied parallel (||) and perpendicular (⊥) to the plane of the AAO template. For pure Co nanowires (Fig. 2a) the magnetic moment at saturation is 10.5±0.1 *memu* and the coercivity in different geometries is $H_c(||)$=330±20 Oe and $H_c(\perp)$=865±30 Oe. The addition of phosphor leads to variation of magnetic properties of Co-based alloy nanowires as shown in Tables 1 and 2. In Fig 2b, the saturation magnetic moment decreases compared with that of pure Co nanowires while the

coercivity significantly increases for both magnetic configurations. Further increase of phosphor content, however, significantly reduces the saturation magnetic moment (to 200±5 *μemu*, which is 50 time smaller than that of Co wires) as well as the coercivity. The perpendicular to plane magnetic anisotropy in conjunction with the high coercivity makes Co-P systems very interesting, not only for high density data storage applications, but also for designing microwave filters, whose absorption bands can be selected as a function of the materials within the arrays [13].

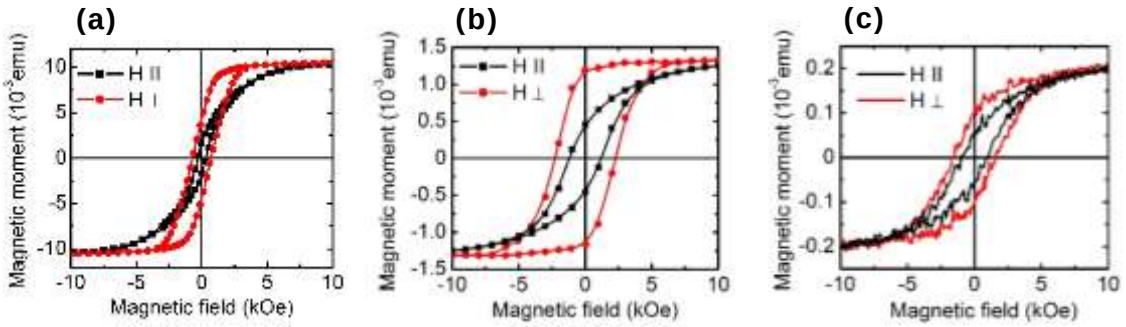

Figure 2 - Room-temperature hysteresis loops measured for arrays of (a) Co, (b) $Co_{93.2}P_{6.8}$ and (c) $Co_{91.8}P_{8.2}$ nanowires electrodeposited in AAO templates using a 15V, 200Hz sinusoidal waveform. ⊥ and || denote perpendicular and parallel directions to AAO substrate.

As seen in Fig.2, for Co and Co-P nanowire arrays the M-H loops exhibit large hysteresis along the parallel and perpendicular directions. All the samples are more easily magnetized along the long axis of the nanowires rather than perpendicular to it due to the strong shape anisotropy. As expected from the theoretical predictions for bulk materials, the saturation field can be defined as $2\pi M_s$, if the shape anisotropy only exists (detailed discussion of the effective anisotropy is given below in the text). For Co and CoP nanowires H_s=8792 Oe (700 kA.m^{-1}) and 5100÷6900 Oe (405÷550 kA.m^{-1}) [14, 15]. This shows that theoretical predictions are consistent with experimental values recorded in Table 1 and Fig.2. The reduction in saturation field with the increase of P content can be attributed to the reduced value of M_s.

As shown in Table 1, the difference in values of H_c(||) and H_c(⊥) for $Co_{93.2}P_{6.8}$ nanowires is much larger than for pure Co nanowires. Assuming that the amorphization of the crystalline structure in

Co-P nanowires and the loss of magnetocrystalline anisotropy is solely responsible for this change in magnetic anisotropy, Co-P nanowires would be expected to exhibit stronger perpendicular to plane magnetic anisotropy than Co nanowires. However, we find that the addition of phosphor does not lead to this outcome.

Table 2 summarizes some data extracted from the magnetic hysteresis loops as well as torque measurements, along with the morphological characteristics of Co and $Co_{93.2}P_{6.8}$ samples. Data for the volume of nanowires, V_w, and saturation moment, m_s, allow us to estimate the saturation magnetization according to $M_s=m_s/V_w$ and compare it with literature values for Co-P alloys. If one knows the magnetic torque L, magnetic material volume V_w and saturation magnetization M_s, then it is possible to estimate the perpendicular magnetic anisotropy field as $H_{a\perp}=2L/(V_wM_s)$ and to compare with $H_{a\perp}$ found from the hysteresis loops using $H_{a\perp}=\int[(M_\perp(H)-M_\parallel(H))/M_s]dH$. Perpendicular magnetic anisotropy constant can be determined as $K_\perp = M_s H_{a\perp}/2$. Various estimates of the magnetization are listed in Table 2 based on different assumptions about the volume occupied by the ferromagnetic nanowires. The influence of the addition of P in Co-P alloys manifests itself in a maximum for H_c and M_r/M_s at x=6.8 wt.% of P. The value of $H_{a\perp}$=3800±200 Oe for $Co_{93.2}P_{6.8}$ nanowires is almost the same as for pure Co wires $H_{a\perp}$=3700±200 Oe. We conclude that $Co_{93.2}P_{6.8}$ nanowires have optimal hysteresis properties for practical applications in data storage and microwave devices, for instance, filters for wireless communication and automotive systems, where a demand exists for smaller sizes and broader bandwidths. The so-called magnetic ‘‘nanowired’’ substrates (MNWS) [16], consisting of nanowires embedded in a porous template, are ideal candidates for this application due to their desirable materials properties and the possibility to build tunable nanomagnetic devices applicable for the desired frequency range [17]. The advantages of Co-P materials compared to classical ferrites are a higher operation frequency, a higher saturation magnetization and resonant frequency, observed without any applied external DC field [18, 19].

Table 2. Experimental magnetic data and morphological characterization for Co and Co-P nanowires.

	Co	$Co_{93.2}P_{6.8}$
saturation moment m_s [emu]	1.10E-02	1.30E-03
torque L [erg]	31.1	2.1
anisotropy field from loops $H_{a\perp}$ [Oe]	3700±200	3800±200
pore diameter d [nm]	30±2	30±2
core diameter D_1 [nm]	30±2	5±1
first shell layer diameter D_2 [nm]	-	20±2
second shell layer diameter D_3 [nm]	-	30±2
porosity ν	0.095	0.095
substrate square S [mm^2]	16±1	12±1
pore volume [cm^3]	7.6E-06	5.70E-06
core volume V_1 [cm^3]	7.6E-06	0.16E-06
first shell layer volume V_2 [cm^3]	-	2.53E-06
second shell layer volume V_3 [cm^3]	-	5.70E-06
M_s of V_1 [Gs]	1450±150	8200±700
M_s of V_2 [Gs]		500±100
M_s of V_3 [Gs]		230±40
M_s (literature) [Gs] Ref[14]		800
M_s (literature) [Gs] Ref [15]	1420	1100
anisotropy field from torque of V_1 [Oe]	5800±800	52000±2000
anisotropy field from torque of V_2 [Oe]		3200±800
anisotropy field from torque of V_3 [Oe]		1400±400

The magnetic properties of nanowires as a function of the addition of P can also be analyzed in the light of the microstructural features of electrodeposited samples. Figure 3 shows TEM images taken from typical Co and $Co_{93.2}P_{6.8}$ samples and the corresponding SAED patterns. For pure Co nanowires we observe a uniform polycrystalline structure, an interpretation supported by the SAED pattern (Fig. 3a). This is consistent with previous report on Co-based alloy nanowires with fine grain polycrystalline nature [20,21]. However, this is not the case for $Co_{93.2}P_{6.8}$ nanowires, when one observes a form of coaxial structure. As seen in Fig. 3b, the wire consists of a core and two shell layers composed of various

materials with different image contrast. The corresponding SAED pattern demonstrates a few bright spots on the halo background, pointing out an existence of the mixture of crystalline and amorphous phases. To estimate M_s for Co and Co-P nanowires, we have calculated the volume occupied by nanowires on a substrate with porosity ν=0.095 as $V_w=LS\nu(D_i/d)^2$, where L=5 μm is the pore length (assumed equal to the nanowire length), S is the substrate area, D_i is the assumed diameter of a ferromagnetic nanowire and d is the pore diameter (30 nm for the samples). As seen in Table 2 for Co nanowires, the experimental value of M_s is in good agreement with literature data, indicating that the pores are fully and uniformly filled with pure Co. The inferred values of anisotropy, measured from hysteresis loops and magnetic torque measurements, are not consistent. This may be because the magnetization reversal for nanowires with this diameter is not limited to coherent magnetization rotation and mainly occurs through the domain wall nucleation and propagation [22-24].

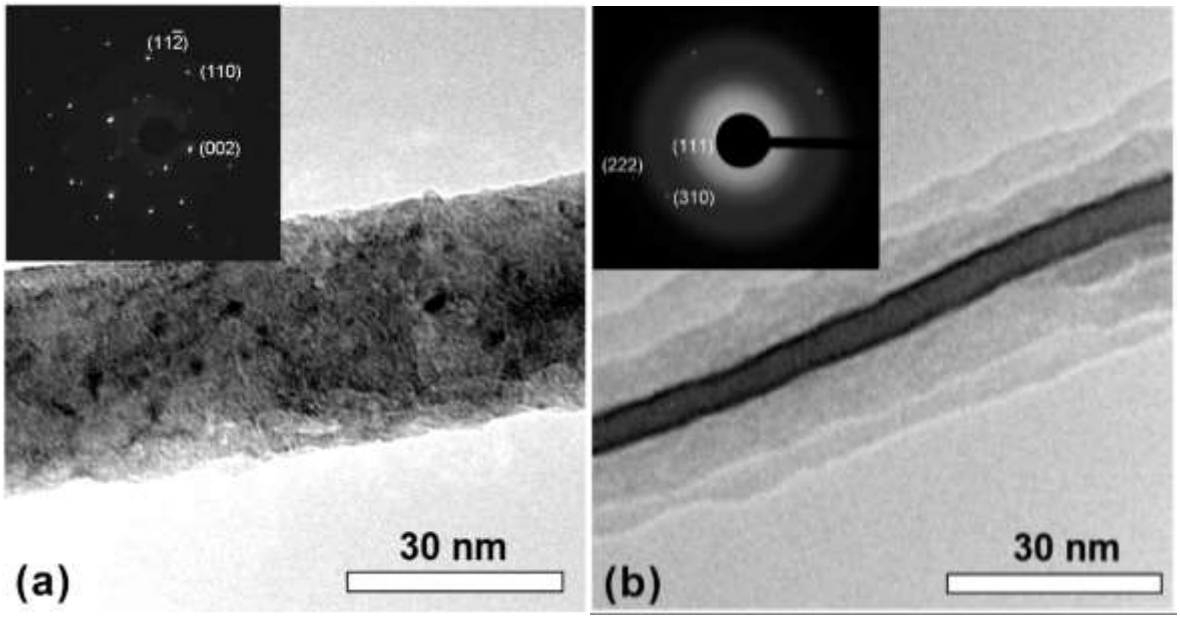

Figure 3 - Typical TEM images and selected area diffraction patterns with main indexes for (a) Co and (b) $Co_{93.2}P_{6.8}$ nanowires electrodeposited in AAO templates using a 15V, 200Hz sinusoidal waveform.

In case of $Co_{93.2}P_{6.8}$ nanowires we assume that the volume V_w of ferromagnetic material is equal to: (1) the volume, V_1, of the core with the actual diameter D_1=5 nm or (2) the volume, V_2, of the core together with the first shell layer having D_2=20 nm or (3) the volume V_3 of the whole coaxial nanowire with D_3=30 nm. We have used these three scenarios for the estimations in Table 2. The first assumption, when $V_w=V_1$, was discarded, because it yielded physically meaningless value M_s ~ 8200 Gs. The value of M_s calculated using an assumption $V_w=V_2$ is closest to the literature data, though still smaller. This might be expected for a coaxial structure where the core has larger magnetization that the first shell layer. In general, the discrepancy between the experimental and literature magnetization indicates that the core and the shell have significantly different magnetizations. Using this method to estimate the volume fraction, the good agreement is observed between the anisotropy field determined from the hysteresis loops and torque measurements. This indicates that magnetization reversal in these nanowires (with a smaller diameter than for Co nanowires with inhomogeneous reversal of the magnetization) is mediated by the uniform (coherent) rotation of the magnetization [24]. It also helps to explain the sharp rise of H_c for Co-P nanowires. On the one hand, CoP nanowires with the smallest P content have the largest fraction of *fcc* phase (which has a large value of magnetocrystalline anisotropy). However, the addition of a small amount of P leads to a decrease of the ferromagnetic core in Co-P nanowires and rendering it much smaller than the pore diameter. If the diameter of NWs is less than the critical diameter for incoherent magnetization reversal (for Co D_{cr} =25 nm, but for Co-P it can vary), then domain wall nucleation becomes an energetically unfavorable process. Thus, the coercivity of Co-P nanowires must be larger than H_c in pure Co nanowires.

Hence our analysis indicates that the core, and the adjacent shell layer, are ferromagnetic, and the outer shell layer is weakly magnetic or possibly nonmagnetic (e,g, Co_2P) as deduced from TEM SAED as discussed above. A few diffraction spots are seen in these core/shell structures which might possibly arise from a crystalline Co_2P phase which has an orthorhombic lattice and is a Pauli paramagnet [25]. We assume that the core consists of a Co-P alloy with a higher saturation magnetization than the first shell

layer, which is possibly a mixture of crystalline and amorphous Co-P phases. For Co-P with x=8.2 and 9.3 wt.% the coaxial structure was still clearly observed, although the core becomes thinner, leading to a reduced nanowire magnetization and coercive field.

As the magnetocrystalline anisotropy of CoP nanowires is weak or even absent due to the presence of an amorphous phase in the crystal structure, there is a simple and reliable method to estimate an effective anisotropy of a nanowire array. This method is based on an assumption that due to the dipolar interaction between nanowires the shape anisotropy of nanowires is reduced by factor (1-3ν), where ν is a porosity of the template [26, 27]. For the self-ordering regimes of pores formation ν is 0.1 [28]. If to assume that for Co-P the effective diameter of magnetic nanowires decreases, than p reduces proportionally to the square diameter. For $Co_{93.2}P_{6.8}$ nanowires the effective diameter of the ferromagnetic core is about 5 nm. It means that ν decreases in 36 times compare to the pure Co nanowires with diameter of 30 nm. As result, the value of 3ν becomes very small. Thus, magnetostatic interaction between $Co_{93.2}P_{6.8}$ nanowires in the array is negligible. This conclusion is supported by the hysteresis loops, which are not significantly sheared as an evidence of the dipolar–dipolar interaction [29].

Conclusion

We have studied the influence of electrodeposition parameters and phosphor incorporation on the structural and magnetic properties of cobalt nanowires. The electrolyte phosphor content influences the growth, microstructure and magnetic properties of nanowires. For the first time, the formation of coaxial Co-P alloy nanowires is demonstrated consisting of a ferromagnetic core and weakly magnetic or even non-magnetic shells, depending on the P content. This conclusion was supported by a careful analysis of magnetization and magnetic anisotropy data. The coercivity of Co-P nanowires is much higher than for pure Co nanowires. Co-P coaxial core-shell nanowire arrays could find applications in magnetic “nanowired” substrates for the realization of novel microwave devices.

Acknowledgments

Alexander Samardak and his colleagues acknowledge the support of the Russian Ministry of Education and Science under NIR 559.2014 and Far Eastern Federal University.

References:

1. F. Nasirpouri, A. Nogaret, Nanomagnetism and Spintronics, World Scientific Pub. Co., 2011.

2. H. Zeng, R. Skomski, L. Menon, Y. Liu, S. Bandyopadhyay, D. J. Sellmyer, *Phys. Rev. B*, **65** (2000) 134426.

3. W. Schwarzacher, D. Lashmore, *IEEE Trans. Magnetics*, **32** (1996) 3113.

4. C. A. Ross, M. Hwang, M. Shima, J.-Y. Cheng, M. Farhoud, T. A. Savas, H. I. Smith, W. Schwarzacher, F. M. Ross, M. Redjdal, F. B. Humphrey, *Phys. Rev. B*, **67** (2002) 144417; also see: C. A. Ross, M. Hwang, M. Shima, H. I. Smith, M. Farhoud, T. A. Savas, W. Schwarzacher, J. Parrochon, W. Escoffier, H. Neal Bertram, F. B. Humphrey, M. Redjdal, *J. Magn. Magn. Mater*., **249** (2002) 200.

5. Paulus P.M., Luis F., Kroll M., Schmid G., de Jongh L.J., *J. Magn. Magn. Mater*., **224** (2001) 180.

6. Kroll M., Blau W.J., Grandjean D., Benfield R.E., Luis F., Paulus P.M., de Jongh L.J., *J. Magn. Magn. Mater*., **249** (2002) 241.

7. Garcıa J.M., Asenjo A., Velazquez J., Garcıa D., Vazquez M., Aranda P., Ruiz-Hitzky E., *J. Appl. Phys.*, **85** (1999) 5480.

8. Strijkers G. J., Dalderop J.H.J., Broeksteeg M.A.A., Swagten H.J.M., Jonge W.J.M., *J. Appl. Phys.*, **86** (1999) 5141.

9. Zeng H., Zheng M., Skomski R., Sellmyer D.J., Liu Y., Menon L., Bandyopadhyay S., *J. Appl. Phys.*, **87** (2000) 4718.

10. Khan H.R., Petrikowski K., *J. Magn. Magn. Mater.*, **249** (2000) 458.

11. Peng Y., Shen T.H., Ashworth B., *J. Appl. Phys.*, **93** (2003) 7050.

12. O. Kazakova, B. Daly, J. D. Holmes, *Phys. Rev. B* **74** (2006) 184413.

13. M. Darques, J. Spiegel, J. De la Torre Medina, I. Huynen, and L. Piraux, *J. Magn. Magn. Mater*., **321**, (2009) 2055.

14. G. Rivero, I. Navarro, P. Crespo, E. Pulido, et al., *J. Appl. Phys*. **69** (1991) 5454.

15. K. Hüller, G. Dietz, R. Hausmann, K. Kölpin, *J. Magn. Magn. Mater*. **53** (1985) 103.

16. J. Spiegel, I. Huynen. *Solid State Phenomena* **389** (2009) 152.

17. C.E. Carreón-González, J. De La Torre Medina, L. Piraux, A. Encinas, *Nano Letters* **11** (2011) 2023.

18. M Darques, J De la Torre Medina, L Piraux, L Cagnon, I Huynen, *Nanotechnology* **21** (2010) 145208.

19. J. De La Torre Medina, J. Spiegel, M. Darques, L. Piraux, I. Huynen, *Appl. Phys. Lett.* **96** (2010) 072508.

20. J. L. Maurice, D. Imho, P. Etienne, O. Durand, S. Dubois, L. Piraux, J. M. George, and P. Galtier, *J. Magn. Magn. Mater.* **184** (1998) 1.

21. F. Nasirpouri, *IEEE Trans. Magnet.* **47** (2011) 2015.

22. L. G. Vivas, M. Vazquez, J. Escrig, S. Allende, D. Altbir, D. C. Leitao, and J. P. Araujo. *Phys. Rev. B* **85** (2012) 035439.

23. D. J. Sellmyer, *J. Phys.: Condens. Matter* **13** (2001) R433.

24. K.R. Pirota, F. Béron, D. Zanchet, T.C.R. Rocha, D. Navas, J. Torrejón, M. Vazquez, M. Knobel, *J. Appl. Phys.* **109** (2011) 083919.

25. H. Hou, Q. Peng, S. Zhang, Q. Guo, Y. Xie, *Eur. J. Inorg. Chem.* **2005** (2005) 2625-2630.

26. V. Vega et al, *Nanotechnology* **23** (2012) 465709.

27. A.S. Samardak et al., *J. Magn. Magn. Mater*. (2014) doi:10.1016/j.jmmm.2014.10.047.

28. K. Nielsch et al, *Nano Letters* **2** (2002) 677.

29. G. Kartopu, O. Yalçın, M. Es-Souni, and A. C. Başaran. *J. Appl. Phys.* **103** (2008) 093915.

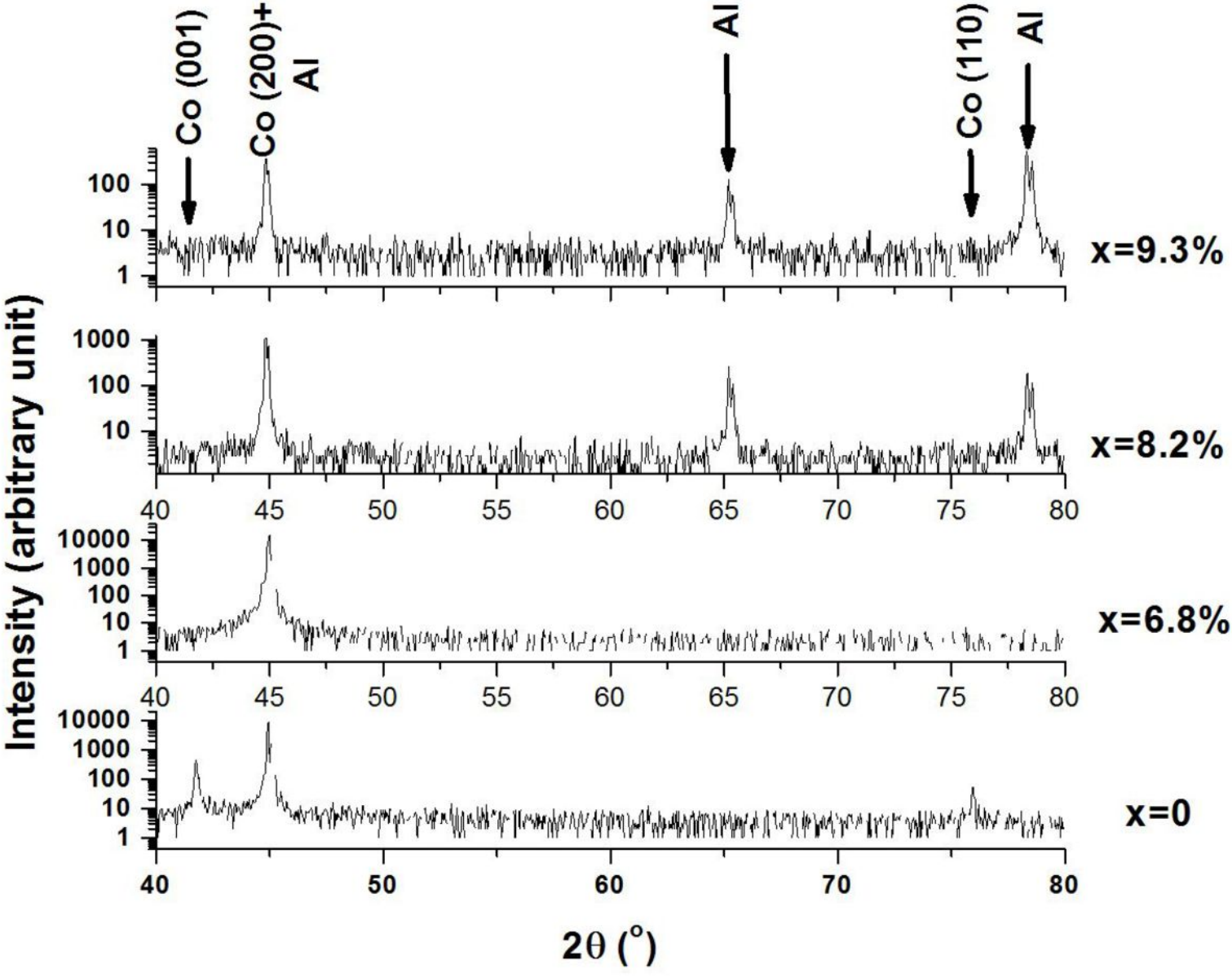
Co (001)
Co (200)+ Al
Al
Co (110)
Al
x=9.3%
x=8.2%
x=6.8%
x=0
Intensity (arbitrary unit)
2θ (°)

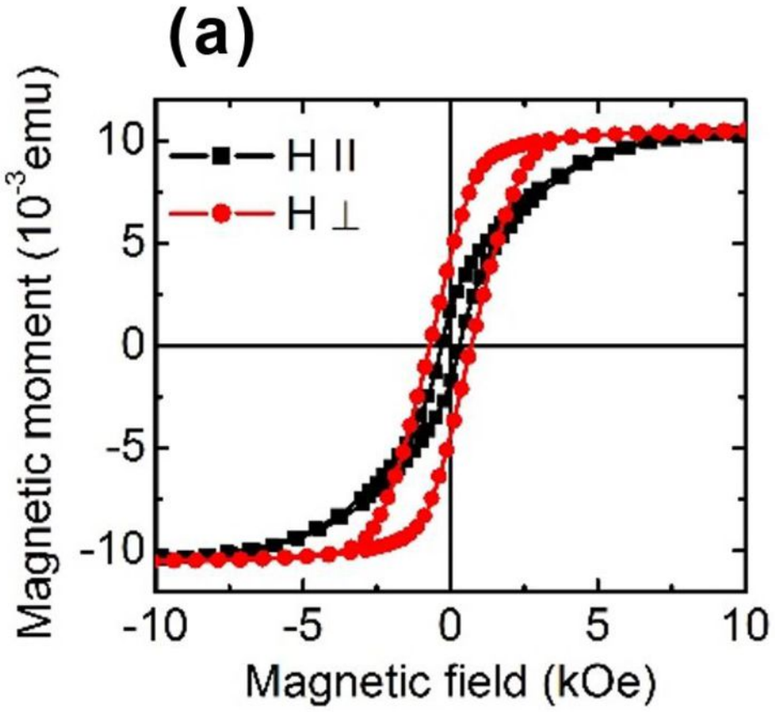
(a)
H II
H ⊥
Magnetic moment (10^{-3}emu)
Magnetic field (kOe)
10
5
0
-5
-10
-10
-5
0
5
10

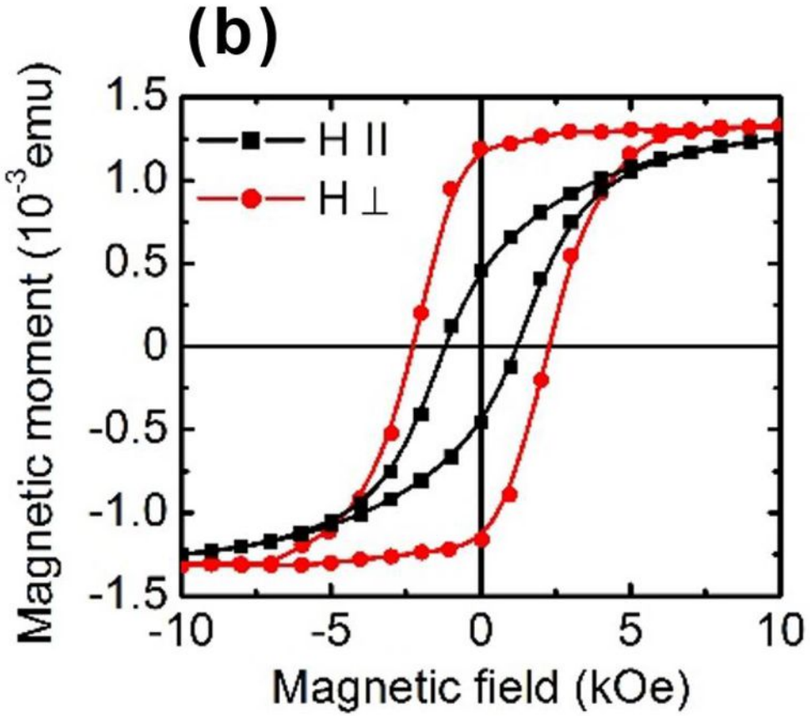
(b)
H II
H ⊥
Magnetic moment (10^{-3}emu)
Magnetic field (kOe)
1.5
1.0
0.5
0
-0.5
-1.0
-1.5
-10
-5
0
5
10

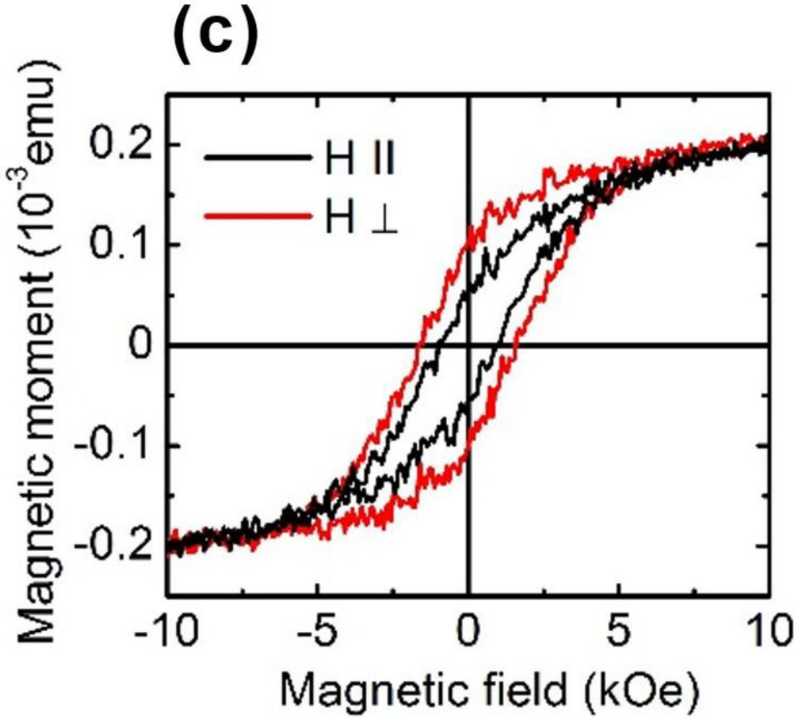
(c)
H II
H ⊥
Magnetic moment (10^{-3}emu)
Magnetic field (kOe)
0.2
0.1
0
-0.1
-0.2
-10
-5
0
5
10

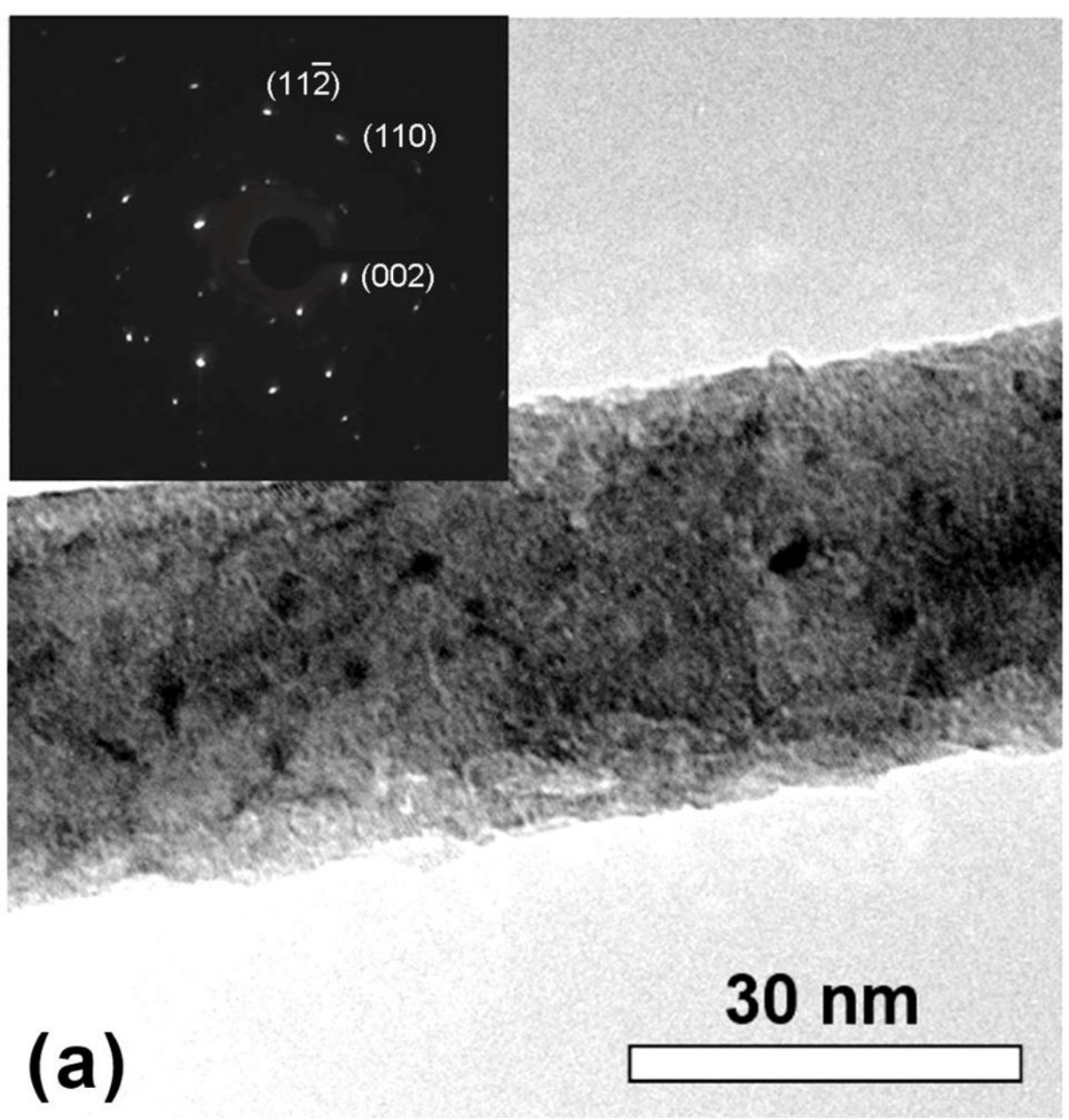
(11$\bar{2}$)
(110)
(002)
30 nm
(a)

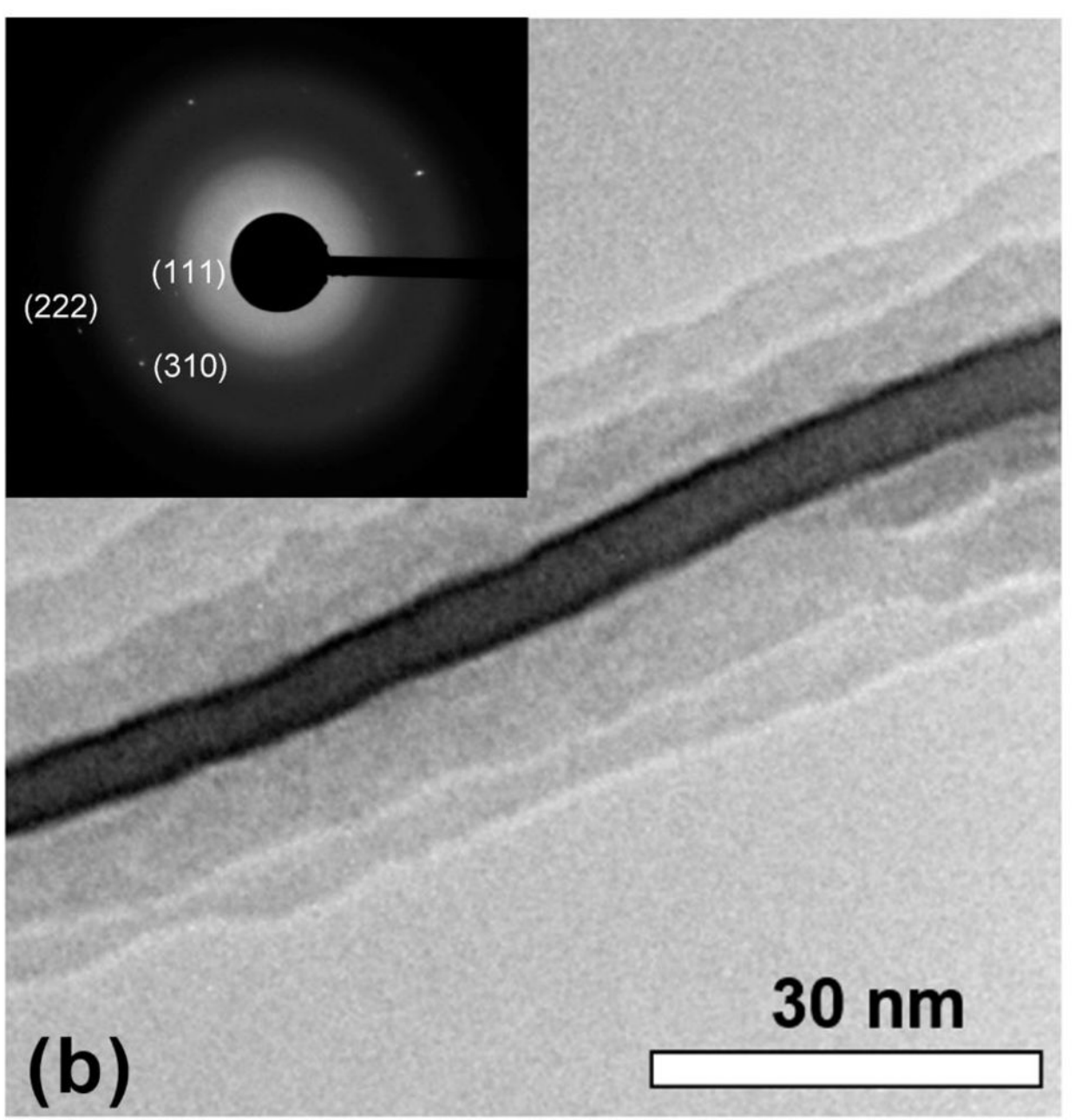
(222)
(111)
(310)
30 nm
(b)